

Mafic enclaves record syn-eruptive basalt intrusion and mixing

Melissa Plail^{1,2}, Marie Edmonds^{3*}, Andrew Woods³, Jenni Barclay¹, Madeleine C.S. Humphreys⁴, Richard A. Herd¹, Thomas Christopher^{5,6}

¹ School of Environmental Sciences, University of East Anglia, Norwich, NR4 7TJ, UK

² School of Geosciences, Witwatersand University, Johannesburg, South Africa

³ Department of Earth Sciences, University of Cambridge, Downing Street, Cambridge, CB2 3EQ, UK

⁴ Department of Earth Sciences, University of Durham, Durham

⁵ Montserrat Volcano Observatory, Montserrat

⁶ Seismic Research Centre, University of the West Indies St Augustine, Trinidad and Tobago W.I.

*corresponding author: marie.edmonds@esc.cam.ac.uk

Abstract

Mafic enclaves hosted by andesite erupted at the Soufrière Hills Volcano between 1995 and 2010 yield insights into syn-eruptive mafic underplating of an andesite magma reservoir, magma mixing and its role in sustaining eruptions that may be widely applicable in volcanic arc settings. The mafic enclaves range in composition from basalt to andesite and are generated from a hybrid thermal boundary layer at the interface between the two magmas, where the basalt quenches against the cooler andesite, and the two magmas mix. We show, using an analytical model, that the enclaves are generated when the hybrid layer, just a few tens of centimetres thick, becomes buoyant and forms plumes which rise up into the andesite. Mafic enclave geochemistry suggests that vapor-saturated basalt was underplated quasi-continuously throughout the first three eruptive phases of the eruption (the end member basalt became more Mg and V-rich over time). The andesite erupted during the final phases of the eruption contained more abundant and larger enclaves, and the enclaves were more extensively hybridised with the andesite, suggesting that at some time during the final few years of the eruption, the intrusion of mafic magma at depth ceased, allowing the hybrid layer to reach a greater thickness, generating larger mafic enclaves. The temporal trends in mafic enclave composition and abundance suggests that basalt recharge and underplating sustained the eruption by the transfer of heat and volatiles across the interface and when the recharge ceased, the eruption waned. Our study has important implications for the petrological monitoring of long-lived arc eruptions.

36 **Keywords:** Mafic enclaves, andesite, arc, mixing, eruption triggering

37

38 **1. Introduction**

39 Andesites are the most common volcanic rock type erupted at convergent margins and are
40 fundamental to the formation and evolution of continental crust (Rudnick, 1995). It is
41 increasingly clear that many intermediate magmas in arcs are hybrids, formed during long
42 residence periods in the crust (Cooper and Kent, 2014) and recharged frequently by mafic
43 magmas (Eichelberger et al., 2000; Reubi and Blundy, 2009). Many intermediate
44 composition magmas erupted in arcs preserve evidence of mingling and mixing with mafic
45 magma shortly prior to eruption in the form of disequilibrium (Nakagawa et al., 2002; Singer
46 et al., 1995; Tepley et al., 1999) or heating textures, diverse isotopic compositions (Davidson
47 and Tepley, 1997; White et al., 2017), the presence of cryptic mafic components (Humphreys
48 et al., 2009b) or macroscopic mafic enclaves (Bacon, 1986; Browne et al., 2006; Clynne,
49 1999; Martin et al., 2006). It remains unclear, however, whether mafic recharge of reservoirs
50 is in itself a trigger for eruption (Murphy et al., 2000; Tepley et al., 1999; Victoria et al.,
51 2008), or an outcome of unrest and impending eruption (Christopher et al., 2015). Such
52 mingled magmas have been erupted at Mount Unzen, Japan (1991-1995) (Browne et al.,
53 2006), Lassen Peak (Clynne, 1999; Tepley et al., 1999), Augustine volcano, Alaska (2006)
54 (De Angelis et al., 2013; Nakamura, 1995), Arenal, Costa Rica (Reagan et al., 1987) and
55 Soufrière Hills Volcano, Montserrat (Murphy et al., 2000).

56

57 Mafic enclaves typically comprise a complex hybrid assemblage of groundmass crystals,
58 residual melt and host magma-derived components, such as “inherited” crystals and melt
59 derived from the host magma (Bacon, 1986; Clynne, 1999; Humphreys et al., 2013;
60 Humphreys et al., 2009b; Plail et al., 2014). Further, host magmas often contain crystals that
61 preserve evidence of their admixture and subsequent ejection from the mafic magma. Thus,
62 suites of cognate enclaves display a range of compositions and textures that reflect variable
63 extents of differentiation of the mafic magma, or the degree of mixing with the host magma
64 and/or changes in end-member magma composition (Bacon, 1986; Browne et al., 2006;
65 Clynne, 1999). While we are making progress in understanding the role of mafic underplating
66 in heating and mobilising magma bodies (Bachmann and Bergantz, 2006; Bergantz et al.,
67 2015; Huber et al., 2011), we lack an overarching understanding of the controls on the nature
68 of mixing with overlying host magmas. It is not known, for example, whether the enclaves
69 reflect quasi-continuous, syn-eruptive mafic underplating, or whether episodes of mafic

70 intrusion are decoupled from eruptions. Host and mafic enclave compositions may evolve
71 during eruptions; these trends might allow understanding of how magmas mingle and on
72 what timescales and what implications this may have for eruption triggering and sustenance.

73

74 There is evidence from a wide range of volcanic systems of magma mixing and mingling
75 between a “host” evolved magma with intruding mafic magma, suggesting this is a common
76 process and integral to the petrogenesis of complex, hybrid andesites. As well as the
77 macroscopic evidence in the form of decimeter-scale mafic enclaves, there is abundant
78 textural and petrological evidence for mixing and mingling. In Soufrière Hills lavas, the
79 presence of plagioclase, pyroxene and oxide microlites, crystal clots, plagioclase phenocrysts
80 with high Fe rims and high K₂O glass derived from the disaggregation of mafic enclaves
81 (Humphreys et al., 2013; Humphreys et al., 2009b), shows that the bulk andesite contains up
82 to 6 % vol. of a ‘cryptic’ mafic component (Humphreys et al., 2013) as well as the 1–12 %
83 vol. in the form of mafic enclaves (Barclay et al., 2010; Komorowski et al., 2010; Mann et
84 al., 2013; Murphy et al., 2000; Plail et al., 2014). In Kanga Island in the Aleutian arc,
85 decreasing andesite bulk SiO₂ concentrations have been correlated with increasing mafic
86 cumulate crystal clots proportions (Brophy, 2009). The 1953-1974 eruption of Trident
87 volcano in Katmai National Park Alaska also shows a decrease in the host dacite bulk SiO₂
88 over the course of the eruption as the storage region homogenises with mafic magma
89 (Coombs et al., 2000). The host magma erupted at Unzen, Japan during the 1991-5 eruption
90 is calculated to contain between 10 and 25 % mafic magma (Browne et al., 2006), which is a
91 result of multiple mixing events (Vogel et al., 2008). The mixing efficiency may change over
92 the course of an eruption caused by gradual changes in bulk viscosity and temperature of the
93 overlying magma, as demonstrated in the 1915 eruption products of Lassen Peak, USA
94 (Clynne, 1999; Klemetti and Clynne, 2014; Sparks and Marshall, 1986). The degree and style
95 of magma mixing can strongly influence eruptive style, as demonstrated by eruptions at
96 Quizapu, Chile (Ruprecht and Bachmann, 2010). The 1846-47 effusive eruption with
97 geochemical and petrological evidence for magma mixing resulted significant reheating of
98 host magma from 830 to 1000 °C; this mixing enhanced magma degassing, but reduced rapid
99 magma expansion and explosive behaviour. Changing mafic enclave compositions over the
100 lifetime of an eruption, where magma mingling is prevalent, have also been observed during
101 many eruptions, but the significance of this is unclear. At Unzen, Japan, the repeated
102 intrusion of two mafic magmas was inferred from differences in REE and trace elements
103 between two distinct mafic enclave types (Vogel *et al.*, 2008). At Shirataka volcano Japan,

104 two mafic enclave types are identified on the basis of high and low K₂O over a 200 kyr
105 period (Hirotsu and Ban, 2006).

106

107 In this paper we present whole rock major and trace element data and glass major element
108 data for andesites and their mafic enclaves erupted during the 1995-2010 eruption of the
109 Soufrière Hills Volcano (Montserrat, West Indies) (Wadge et al., 2014). This well-studied
110 eruption produced magma mixing and mingling features that are common to many
111 intermediate arc magmas globally. The data are used to infer the petrogenesis of the enclaves
112 and to develop an analytical model to describe the formation of the enclaves from a mixed
113 boundary layer at the interface between mafic magma and overlying andesite. The temporal
114 trends in composition are used to assess whether basalt was intruded in a discrete event at the
115 beginning of the eruption, or quasi-continuously throughout, and whether enclave
116 compositions might be useful for evaluating whether long-lived eruptions may be waning.

117

118 *1.1 Geological setting*

119 Most of the volcanic centres on Montserrat (West Indies; **Figure 1**) are andesitic, with mafic
120 enclaves ubiquitous in the lava domes and block and ash deposits. South Soufrière Hills
121 Volcano, which abuts Soufrière Hills at the south of the island (**Figure 1**) has erupted
122 magmas of basaltic to basaltic andesite composition (Cassidy et al., 2015; Zellmer et al.,
123 2003a). The recent eruptions of Soufrière Hills included five phases of andesitic dome-
124 forming activity, separated by pauses in lava extrusion (**Table 1**) (Wadge et al., 2014),
125 allowing examination of temporal trends in magma composition. Samples of andesite and
126 mafic enclaves emplaced during phases III, IV and V were collected at locations shown in
127 **Supplementary Table 1**. Data for phases I and II are compiled from the literature (Mann et
128 al., 2013; Murphy et al., 2000; Zellmer et al., 2003a).

129

130 Previous work has characterised the andesite and its mafic inclusions. The complex zoning
131 patterns and disparate age histories of plagioclase phenocrysts indicate that the andesite is a
132 hybrid that has undergone multiple cooling and reheating events in the shallow crust for 10³–
133 10⁴ years prior to the current eruption (Zellmer et al., 2003a; Zellmer et al., 2003b). Excess
134 sulfur emissions, mafic enclaves and phenocryst disequilibria textures (Barclay et al., 1998;
135 Edmonds et al., 2001; Humphreys et al., 2009b; Murphy et al., 2000; Murphy et al., 1998;
136 Sparks et al., 1998) are interpreted as evidence of an intrusion of a hotter, volatile-saturated
137 mafic magma at depth underplating the andesite (Christopher et al., 2010). Remobilisation

138 and reheating of the crystal-rich andesite has been proposed to have been initialised via
139 ‘convective self-mixing’, ‘gas sparging’ or ‘a defrosting front’ (Bachmann and Bergantz,
140 2006; Burgisser and Bergantz, 2011; Couch et al., 2001). Diffusion profiles across Fe-Ti
141 oxides in the andesite constrain the timing of the interaction between mafic and andesitic
142 magmas to be days to weeks before eruption (Devine et al., 2003). Seismic “crises” which
143 occurred prior to the onset of the 1995-2011 eruption and in 1933-7 and 1966-7 (Shepherd et
144 al., 1971) have been proposed to have been caused by magma intrusion at depth (Aspinall et
145 al., 1998).

146

147 The volume fraction of mafic enclaves in the erupted andesite has increased from ~1% in
148 phase I to ~8-12% in phase V (Barclay et al., 2010; Komorowski et al., 2010; Murphy et al.,
149 2000; Plail et al., 2014), but the causes for this are enigmatic. Substantial quantities of mafic-
150 derived material are also found disaggregated at the crystal-scale within the andesite
151 (Humphreys et al., 2013). Mafic enclaves have become larger with time: 87% of 158 phase I
152 hybrid enclaves observed in the field were under 6 cm in longest dimension (Plail et al.,
153 2014). In phase III, the maximum size for an enclave measured was 14 cm (Barclay et al.,
154 2010). The largest phase V enclave measured to date is 26 cm.

155

156 **2. Samples and Methods**

157 Samples of lava dome blocks containing mafic enclaves were acquired from block and ash
158 deposits erupted during phases III to V (details of sampling locations and deposit types are
159 given in **Supplementary Material**). Splits of samples were crushed and powdered and
160 blocks were also made into 30 micron thick probe sections. Seventy-four powders from mafic
161 enclave and andesite samples were analysed using X-ray fluorescence (XRF) (details of
162 methods and precision are given in **Supplementary Material**). Glasses in the groundmass of
163 mafic enclaves and andesite samples were analysed using a Cameca 5-spectrometer SX-100
164 electron probe at the University of Cambridge (details of operating conditions and standards
165 are given in **Supplementary Material**).

166

167 **3. Results**

168 *3.1. Host andesite geochemistry*

169 The andesite lavas from Soufrière Hills Volcano have a narrow range of bulk compositions
170 (58–63 wt % SiO₂), and are highly porphyritic, with 45-55% macrocrysts (Barclay et al.,
171 1998; Devine et al., 1998; Humphreys et al., 2009b; Murphy et al., 2000) (**figure 2**). The

172 macrocryst assemblage is predominantly plagioclase, hornblende, orthopyroxene and Fe-Ti
173 oxides (ilmenite and magnetite). The groundmass assemblage is plagioclase, orthopyroxene,
174 clinopyroxene and Fe-Ti oxides, with variable amounts of rhyolitic glass (Humphreys et al.,
175 2010; Humphreys et al., 2009b). Soufrière Hills Volcano andesite falls in within the calc-
176 alkaline field (Miyashiro, 1974) (**figure 2**). Major element covariation plots display linear
177 trends (**figure 2**). Matrix glass in the andesite is of rhyolitic composition, with 73–80 wt %
178 SiO₂ (**figure 2**) and variable K₂O, FeO and TiO₂ concentrations (Humphreys et al., 2010).
179 Trace element profiles are shown in **figure 3** and show, in general, enrichments in the large
180 ion lithophile elements (LILE) Rb, K and Ba, and depletions in the high field strength (HFS)
181 elements Ti, Nb and Ta and a trough-like pattern in the MREE to HREE. Covariation plots of
182 trace elements display linear trends (**figure 4**): Dy and Yb increase with increasing La,
183 whereas V, Sr and Sc decrease with increasing La.

184

185 3.2. *Mafic enclave geochemistry*

186 Mafic enclaves have a diktytaxitic groundmass framework of elongate, randomly-oriented
187 crystals indicative of quench crystallisation (**figure 1**). The groundmass consists of
188 plagioclase, clinopyroxene, amphibole, orthopyroxene and Fe-Ti oxides. Variable amounts of
189 interstitial rhyolitic glass are found within the enclaves. ‘Inherited’ phenocrysts of
190 plagioclase, amphibole and orthopyroxene derived from the andesite are present within the
191 mafic enclaves with sieve textures and morphologies typical of those within the host andesite
192 (Humphreys et al., 2009b; Plail et al., 2014).

193

194 The mafic enclaves have a wide range of bulk rock compositions (48–57 wt % SiO₂) (**figure**
195 **2**) and they fall in the tholeiite field (Miyashiro, 1974) (**figure 2**). The suites of mafic enclave
196 compositions from all eruptive phases fall on linear arrays (that include the andesite
197 compositions) for the major elements (**Figure 2**). Trace element profiles show, similar to the
198 andesite, LILE enrichment and HFS element depletion (**figure 3**). Overall, the mafic enclave
199 trace element concentrations are more depleted relative to the host andesite in the LILE and
200 some light REE (La to Pr) (**figure 3**), but there is either enrichment in or overlap with the
201 andesite concentrations in middle REE (Nd, Sm, Eu) the heavy REEs (Dy to Lu) and Zr.
202 Covariation plots of trace elements with La are linear, where Dy and Yb increase whereas V,
203 Sr and Sc decrease with increasing La (**Figure 4**). Similar to the andesite, most of the trace
204 elements and in particular elements such as Sm, Y, Yb, V, Sc show displacements in
205 composition between eruptive phases (V and Yb against La are shown in **Figure 4**), with

206 earlier eruptive phases richer in Dy, Yb and incompatibles and poorer in V, Sc. Correlation
207 coefficient analysis (R, using the corrcoeff function; **Supplementary Material**) shows that
208 trace elements across the eruptive phases correlate positively with one other apart from the
209 Fe-Mg-Ca-Al-V-Ti group, which correlate negatively with all other elements.

210

211 The glass in the mafic enclaves is rhyolitic (70–79 wt% SiO₂) (**figure 2**) with variable K₂O,
212 FeO, TiO₂, SiO₂, CaO and MgO contents, with considerable overlap between mafic enclave
213 and andesite glass compositions (**Figure 2**) (Humphreys et al., 2010). Some mafic enclave
214 glasses have anomalously low Na₂O and overall, glass in the mafic enclaves has higher TiO₂
215 (and lower CaO contents) than the glass from the andesite (**Supplementary Material**).

216

217 3.3. *Temporal variations in magma composition and petrography*

218 Although overall the major, trace and rare earth element patterns of mafic enclaves are
219 similar throughout the eruption, there are changes in the composition of the enclaves and,
220 albeit to a lesser extent, the host andesite, through time (**figure 5**). Host andesite major
221 element compositions show minor displacements in FeO_{tot} and MgO at a fixed SiO₂, with
222 andesite erupted in phases I to II more Fe-rich and Mg-poor than phases III and V andesite
223 (Christopher et al., 2014). These changes are manifest most clearly as a change of 0.5 to 1.0
224 in FeO_{tot}/MgO in both andesite and mafic enclaves at a fixed SiO₂ (**figure 2E**) and in plots of
225 Mg/Fe and V/La with time (**figure 5**). The compositional gap in SiO₂ between the mafic
226 enclaves and the andesite (between 55.5 and 57.5 wt%) observed in phases I-III no longer
227 exists in phase V, with enclave and andesite compositions overlapping (**figure 2**; Plail et al,
228 2014). The SiO₂ content of the host andesites extends to a higher upper range in phases IV
229 and V than in phase I (**figure 5**). The mean SiO₂ content of the mafic enclaves increases
230 towards the end of the eruption: phase I enclaves have on average 52.4 wt% SiO₂ (with a
231 standard deviation of 2 wt%), compared with a mean of 54.0 wt % SiO₂ for phase V enclaves
232 (with a standard deviation 1.6 wt%). The most evolved phase I enclave has 54.7 wt% SiO₂,
233 whereas the most evolved enclave erupted in phase V has 57.2 wt% SiO₂.

234

235 Mafic enclave bulk MgO and FeO compositions (at a fixed SiO₂ content), and to a lesser
236 extent TiO₂ and Al₂O₃, are displaced between phases I to II to III and IV in the mafic
237 enclaves (Barclay *et al.*, 2010) (**figures 2, 5**). Mafic enclaves erupted in phases III and V
238 have systematically higher concentrations of V and Sc and lower concentrations of Y relative
239 to those erupted during phases I and II (**Figure 4, 5**). High field strength elements such as Zr,

240 Hf, Th and U have relatively constant concentrations in the mafic enclaves through the
241 eruptive phases. There is also no variation in the Ba/La and Th/La ratios of mafic enclaves
242 (**Supplementary Material**). Primitive mantle-normalised REE profiles show steepening
243 from phases I to III to V (**Figure 3**) as LREE/MREE ratios increase from phase I (La_N/Sm_N
244 1.0–1.8) to phase 5 ($La_N/Sm_N = 1.5–2.4$). In the more differentiated enclaves, the MREE
245 (Sm, Eu, Gd, Tb, Dy) are enriched relative to the andesite in phases I to III, but form co-
246 linear arrays with the andesite in phase V (**Supplementary Material**).

247

248 **4. Discussion**

249 In summary, the mafic enclaves within the andesite at Soufrière Hills Volcano are basaltic to
250 basaltic andesite in bulk composition, with trace element patterns typical of subduction-
251 related magmas. We show in this section that mixing between a basalt end member and the
252 overlying andesite controls the mafic enclave compositions (**Figures 2-5**). Over time, the end
253 member basalt became slightly more Mg-rich (and Fe-poor) between phases I and III, with
254 associated enrichments in MREE and HREE, suggesting continual recharge of the
255 underplating basaltic layer (as this trend cannot be explained by in situ fractional
256 crystallisation of the basalt beneath the hybrid layer). The geochemical and petrological data
257 are used to develop a model to describe how mafic enclaves form due to the formation of
258 buoyant plumes formed in a hybridised boundary layer at the interface between the two
259 magmas, its thickness controlled by thermal diffusion and magma density. We suggest, based
260 on the temporal changes in abundance and size of the enclaves through the eruption, and the
261 more silica-rich nature of the enclaves erupted in phase V, that basaltic recharge may have
262 ceased sometime after phase III, allowing thickening of the hybridised boundary layer
263 between the magmas by thermal diffusion and generation of larger, more hybridised
264 enclaves.

265

266 *4.1. Hybridization between host andesite and intruding mafic magma*

267 First we demonstrate that the range in mafic enclave compositions is not well explained by
268 fractional crystallisation. We use RhyoliteMELTS (Ghiorso and Gualda, 2015) to construct
269 fractional crystallisation trends for the most primitive mafic enclave composition (at water
270 contents of 4 and 6 wt% (Barclay et al., 1998; Edmonds et al., 2014; Humphreys et al.,
271 2009a), pressure of 150 MPa and fO_2 of QFM and QFM+2 (Devine et al., 1998)(shown on
272 **Figure 2**), similar to the analysis by Cassidy et al., (2015). The geochemical trends in the
273 mafic enclave arrays cannot be produced by fractional crystallisation of a mafic end member

274 melt (**figure 2**), unless a very high oxidation state is invoked, which is not consistent with
275 petrological constraints (Devine et al., 1998; Murphy et al., 2000). Furthermore, the
276 systematic straight-line trends instead suggest that mixing is the dominant control on the
277 major element geochemistry of the enclaves.

278 The presence in the mafic enclaves of phenocrysts inherited from the andesite (Murphy *et al.*,
279 2000; Zellmer *et al.*, 2003a; Barclay *et al.*, 2010; Humphreys *et al.*, 2009; Mann 2010; Plail
280 *et al.*, 2014; Humphreys et al., 2013) is further evidence for physical mixing between the
281 mafic and andesitic magmas, indicating that the mafic enclaves have undergone hybridisation
282 with the andesite. Co-linear trends in major elements between the mafic enclaves and
283 andesite suggest that simple mixing can resolve the range of compositions across the eruptive
284 phases (**Figures 2, 4**), as well as the loss of the compositional gap between the andesite and
285 mafic enclaves in phase V (**Figure 2**). The range in types of mafic enclave erupted in phase
286 V has been explained previously by differing degrees of interaction between a mafic end
287 member and the andesite bulk composition (Plail et al., 2014). “Type A” enclaves are basaltic
288 with a narrow range of compositions (~49–52 wt % SiO₂), and have chilled margins, high-Al
289 amphiboles, a higher glass fraction, high vesicularity and low inherited phenocryst
290 abundance. These are interpreted to be closest in composition to the underplating mafic
291 magma end member composition. The more abundant “type B” enclaves have a broad range
292 of compositions (53–57 wt % SiO₂), and are identified by a lack of chilled margins, a lower
293 glass fraction, low vesicularity and high inherited phenocryst abundance (~25%), and rare to
294 absent high-Al amphiboles; these enclaves are interpreted to have been affected most by
295 mixing with the overlying andesite. As well as type A and B, there are also composite
296 enclaves in andesites erupted during phase V, which comprise a vesicular basaltic core,
297 surrounded by more evolved magma (Plail et al., 2014).

298 Major element mixing (see **Supplementary Material for calculations**) between the phase V
299 andesite (MVO1538-b) and the mafic magma type A end-member (MT27) show that a high
300 percentage (67%) of andesite magma is required to achieve the most evolved type B mafic
301 enclave composition (MT25). This amount of mixing fits the distributions of most trace
302 elements (**figure 4, mixing lines**), with a Σr^2 of 0.2, with the exception of Sm, Tb, Dy, Ho
303 and Er (**Supplementary Material**). The 2:1 bulk rock mixing ratio is also qualitatively
304 consistent with the observed high percentage of inherited phenocrysts (15–25 %) in the type
305 B enclaves, and undoubtedly also a proportion of rhyolitic melt from the andesite must have
306 been mixed into the mafic magma during phenocryst incorporation.

307 Systematic variations that may be explained by mixing are also observed in the glass
308 compositions in the enclaves, in particular in K₂O, FeO and TiO₂ content (Humphreys *et al.*,
309 2010; Devine *et al.* 2014; Humphreys *et al.* 2015). Phase V type A enclave glasses contain
310 high K₂O, TiO₂, and FeO rhyolitic concentrations compared to the type B enclave glass
311 compositions which overlap with the host andesite matrix glasses (Humphreys *et al.*, 2015).
312 Textural observations indicate that, upon intrusion into the andesite, quench-crystallisation of
313 the mafic magma occurred *in situ* involving an assemblage of plagioclase, ±amphibole,
314 ±clinopyroxene and magnetite. Using a simple assemblage of plagioclase 80 % and
315 amphibole 20 %, to represent roughly the appropriate modal proportions of a type A enclave
316 diktytaxitic framework assemblage, a rhyolitic melt of ~76 wt% SiO₂ can be generated after
317 ~58 % crystallisation from the phase V mafic end-member composition (from
318 RhyoliteMELTS). Varying the modal proportions of the framework assemblage and
319 substituting clinopyroxene for amphibole, this amount of crystallisation would generate a
320 range of melt compositions (~70–80 wt% SiO₂) that fits the observed range in the enclaves.
321 Although this model is a good fit for SiO₂ it does not resolve the full range of compositional
322 differences in K₂O, TiO₂ and FeO between the enclaves. Instead, the overlap between the
323 enclave and host andesite matrix glasses compositions (**Figure 2**) may be evidence for the
324 mixing of heterogeneous melts during enclave formation at the interface between the two
325 magmas (Laumonier *et al.*, 2014). The andesite matrix glass has also been shown to be highly
326 heterogeneous with respect to K₂O, consistent with mingling of melts, with the variable
327 diffusion kinetics of K and Ti producing a spread in concentrations (Humphreys *et al.*, 2010).

328

329 4.2. *Temporal changes in composition and abundance of mafic enclaves through the* 330 *eruption*

331 There are clear changes in enclave geochemistry through the eruption. Displacements in Fe,
332 Mg and V, Yb (and other MREE and HREE) concentrations are observed between enclaves
333 erupted during the different phases (**Figures 2, 4, 5**). There was also a small increase in the
334 andesite temperature between phases I and V by 10 °C, inferred from Fe-Ti oxide
335 geothermometry, (Devine & Rutherford, 2014), consistent with heating by basaltic
336 underplating below.

337

338 We have established in the previous section that the colinear trends in the mafic enclaves are
339 the result of mixing. Displacements in elemental composition for a fixed SiO₂ or La
340 composition may be explained by changes in the composition of the end member basalt with

341 time. In order to explain the enrichment in MgO and V in the end member mafic magma
342 between phases I and III (**figure 5**), we invoke intrusion of slightly more primitive magma
343 with time. This change in end member magma composition between phases I and III is good
344 evidence for sustained and continuous replenishment of the underplating basaltic layer during
345 this time (up to 2008; **figure 5**). The presence of larger and more abundant enclaves in phase
346 V (Barclay et al., 2010; Komorowski et al., 2010) suggests perhaps that a boundary layer
347 between the magmas changed in dimension, thickening and cooling, which would be
348 consistent with the supply of mafic magma having ceased some time after phase III. We will
349 explore this idea further in the next section, where we develop an analytical model.

350

351 *4.3. The evolution of the interface between underplating mafic magma and andesite*

352 The interaction between a cooler evolved andesite above a hot basaltic melt intrusion
353 involves heat transfer from the basalt to andesite. Initially the heat transfer is governed by
354 thermal conduction in both layers, with crystals in the partially crystalline andesite melting,
355 while the cooling basalt gradually crystallises. There is an abundance of evidence in the
356 andesite for heating and partial melting: sieve textures in the plagioclase (Humphreys et al.,
357 2009b; Murphy et al., 2000), resorbed phenocrysts of orthopyroxene (with reversely zoned
358 overgrowths or overgrowths of clinopyroxene) (Humphreys et al., 2009b; Murphy et al.,
359 2000), quartz either strongly resorbed or jacketed by clinopyroxene crystals (Humphreys et
360 al., 2013; Murphy et al., 2000) and hornblende surrounded by thermal reaction rims
361 (Humphreys et al., 2009a; Rutherford and Devine, 2003) are all present. Owing to the
362 different composition and solidus temperatures of the basalt and andesite, the andesite near
363 the interface with the basalt may become fully molten if the basalt is sufficiently hot. In the
364 diffusive boundary layers, the bulk density of the magmas gradually changes. In particular,
365 the bulk density of the andesite typically decreases as the relatively dense mineral phases
366 melt, while the bulk density of the basalt initially increases on cooling and crystallisation.
367 However, if the basalt becomes vapor-saturated then on continued cooling, the basalt will
368 exsolve volatiles, leading to a gradual decrease in the bulk density. Eventually, the basalt may
369 become less dense than the overlying andesite and small plumes of volatile-laden basalt may
370 rise into the andesite. Since the andesite in the thermal boundary layer is hotter than the
371 overlying layer, this layer will become much less viscous through both reduction in the
372 crystal content and also heating of the melt. As a result, the plume rise within the boundary
373 layer will occur more rapidly than the mixing into the overlying cooler layer of andesite, so
374 that the basalt and andesite intermingle only on the scale of the boundary layer.

375 Subsequently, as the thermal boundary layer becomes deeper, this buoyant intermingled layer
376 may rise up into the main body of andesite, forming hybrid mafic enclaves consisting of a
377 mixture of basalt and the heated andesite from the boundary layer, just as is observed in the
378 geochemical data (**figures 2-4**).

379

380 Although the process is a continuum, we present a series of calculations in which we model
381 the temperature evolution of the boundary layer in the limit that thermal conduction governs
382 the heat exchange until the point at which plumes of buoyant basalt, bearing exsolved
383 volatiles, rise up into the heated boundary layer of andesite. We then estimate the thickness of
384 the bulk thermal boundary layer at the point that it can rise into the overlying main body of
385 andesite, which has much higher viscosity than the boundary layer. Although the calculations
386 are simplified they provide some insight into the possible process of intermingling within the
387 local boundary layer, which can occur more quickly than the rise of basaltic enclaves into the
388 main body of andesite, and which leads to the enclaves consisting of a mixture of remelted
389 andesite mixed with the basalt, as seen in the samples discussed here.

390

391 We model the crystal fraction of the basalt and the andesite as following laws of the form
392 $X_s(T)$ and $X_b(T)$, so that the temperature above ($z>0$) and below ($z<0$) the interface ($z=0$)
393 is given by the thermal diffusion equation

394

$$395 \left[\rho C_p + \rho L \frac{dX_i}{dT} \right] \frac{\delta T}{\delta t} = k_i \frac{\delta^2 T}{\delta z^2} \quad (1)$$

396

397 where i denotes the basaltic (b) or andesitic (s) melt and k_i is the thermal conductivity of the
398 basalt or andesite. In modelling X_b and X_s we use the approximate linearised laws:

399

$$400 \begin{aligned} X_b(T) &= 0.02(1200 - T) \\ \text{and} \\ X_s(T) &= 0.035(972 - T) \end{aligned} \quad (2)$$

401

402 obtained by linear approximation to calculations carried out using the program Melts
403 (Ghiorso and Sack, 1995). Here $T_m = 972$ °C is the temperature at which the andesitic magma

404 is purely molten, with no crystal phase, while $T_b = 1200$ °C is the temperature at which the
 405 basalt is purely molten. These linearised relations are useful since they lead to analytical
 406 solutions for the thermal diffusion equation (1), as presented below.

407

408 In our calculations, we assume that the latent heat of crystallisation has value $L = 7.42 \times 10^5$
 409 J/kg, with $\rho = 2500$ kg/m³ and $C_p = 1000$ J/K/kg. We assume the initial temperature of the
 410 basalt is $T_b = 1200$ °C on injection into the magma chamber, while the andesite has initial
 411 temperature $T_s = 835$ °C. Two pyroxene thermometry in mafic enclaves yields temperatures
 412 of 1,074–1,196° C (n = 5) (Humphreys et al., 2009b). QUILF (Andersen et al., 1993) used in
 413 single-pyroxene mode (Murphy et al., 2000) gave typical orthopyroxene phenocryst core
 414 temperatures of 800–900° C (average 850° C, n = 77). Phenocryst rims are typically slightly
 415 hotter (average 870° C, n = 61). Temperature estimates were also obtained using the
 416 hornblende- plagioclase geothermometer of (Holland and Blundy, 1994). One phenocryst
 417 pair gave a temperature of 844° C. The interface temperature, T_i between the basalt and the
 418 andesite is then given by the continuity of heat conduction across the interfaces. Using the
 419 above values for the properties of the melt, we find that the interface temperature is predicted
 420 to have value $T_i \sim 1008$ K $> T_m$ (see below), so that immediately above the interface the
 421 andesite is purely molten. The thermal diffusivity of the melt layer of andesite has value:

422

$$423 \quad \kappa_m = \frac{k}{\rho C_p} \quad (3)$$

424

425 In contrast, in the basalt and the cooler region of the andesite, in which there is a crystal
 426 phase present, the effective thermal diffusivity accounts for the thermal buffering associated
 427 with the latent heat, leading to the relation

428

$$429 \quad \kappa_i = \frac{\left[\rho C_p + \rho L \frac{dX_i}{dT} \right]}{\rho C_p} \quad (4)$$

430

431 for the basalt ($i = b$) and the silicic ($i = s$) melt when partially crystalline. With these three
 432 regions of partially crystalline basalt in the region $z < 0$, the molten andesite in the region 0

433 $z < a(t)$ and the partially molten andesite in the region $z > a(t)$, then prior to the onset
 434 of convection, we find the approximate diffusive temperature profile

$$435 \quad T(z, T) = T_I + (T_b - T_I) \operatorname{erf} \left[\frac{-z}{\sqrt{(\kappa_b t)}} \right] \text{ for } z < 0 \quad (5)$$

$$436 \quad T(z, T) = T_I + (T_m - T_I) \frac{\operatorname{erf} \left[\frac{z}{\sqrt{(\kappa_m t)}} \right]}{\operatorname{erf} \left[\frac{a(t)}{\sqrt{(\kappa_m t)}} \right]} \text{ for } a(t) > z > 0 \quad (6)$$

437

$$438 \quad T(z, T) = \frac{T_m \left(1 - \operatorname{erf} \left[\frac{z}{\sqrt{(\kappa_s t)}} \right] \right) - T_s \left(1 - \operatorname{erf} \left[\frac{a(t)}{\sqrt{(\kappa_s t)}} \right] - \operatorname{erf} \left[\frac{z}{\sqrt{(\kappa_s t)}} \right] \right)}{1 - \operatorname{erf} \left[\frac{a(t)}{\sqrt{(\kappa_s t)}} \right]} \text{ for } z > a(t) \quad (7)$$

439

440 where the interface temperature T_I is given by continuity of heat flux across the
 441 interface

442

$$443 \quad T_I = \frac{T_m + T_b \beta \operatorname{erf}(\lambda)}{1 + \beta \operatorname{erf}(\lambda)} \text{ where } \beta = \left(\frac{\kappa_m}{\kappa_b} \right)^{1/2} \text{ and } \lambda = \frac{a(t)}{(\kappa_m t)^{1/2}} \quad (8)$$

444

445 where the location of the pure melt front in the andesite, $z = a(t)$, is given by the solution for
 446 λ of the equation

447

$$448 \quad \gamma (1 + \beta \operatorname{erf}(\lambda)) \exp(-\lambda^2 \gamma^2) (T_m - T_s) = \exp(-\lambda^2) (1 - \operatorname{erf}(\lambda \gamma)) (T_b - T_m) \quad (9)$$

449

450 with

$$451 \quad \gamma = (\kappa_m - \kappa_s)^{1/2} \quad (10)$$

452

453 In **figure 6A**, we show a calculation of the structure of the thermal boundary layers across the
454 interface, calculated after 1 and 10 days. After about 1 day, the thermal boundary layer
455 extends about 10-20 cm into the andesite and basalt, while after 10 days, the boundary layer
456 has grown to a thickness of >60 cm.

457

458 In calculating the potential for convective overturn within this boundary layer, we note three
459 key effects. First, the andesite has a much reduced crystal fraction in the boundary layer
460 leading to a reduction in the viscosity by a factor of 10-100, from values of order 10^5 to 10^6
461 Pa s, to 10^3 to 10^4 Pa s, while the viscosity of the basaltic layer increases from values of 10-
462 100 Pa s to 10^3 to 10^4 Pa s in the cooled region of the boundary layer. Also as the basalt
463 crystallises, it will tend to become saturated in volatiles at a particular crystal content. As
464 volatiles are exsolved, the density of the basaltic melt gradually decreases. The decrease in
465 density depends on the volatile content of the magma, but will typically be of order 10-150
466 kg/m^3 (Phillips and Woods, 2002). The solubility of water in the melt can be approximated
467 by Henry's law, $n_d = sP^{1/2}$ and so with a crystal content X the mass of exsolved volatiles is
468 given by

469

$$470 \quad n_e \sim n_0 - sP^{1/2}(1 - X) \quad (11)$$

471

472 where n_0 is the total volatile content of the basalt. This leads to an effective bulk density of
473 the bubble-melt mixture given by

474

$$475 \quad \rho = \left[\frac{n_e}{\rho_g} + \frac{1 - n_e}{\rho_m} \right] \quad (12)$$

476

477 where ρ_g and ρ_m are the gas and melt densities. With a total volatile mass fraction in the
478 range $n_0 = 0.02 - 0.04$ and a crystal fraction in the range $X = 0.2 - 0.4$ the melt density is
479 typically $10-200 \text{ kg/m}^3$ lower than the andesite (**figure 6B**). These approximate calculations
480 based on this simplified parameterised Henry's law with magma of total volatile content
481 (mass fraction) 0.02 (green) and 0.04 (red) are consistent in magnitude with full numerical

482 calculations using Melts (Woods and Cowan, 2009). As this boundary layer of cooled basalt
 483 becomes less dense than the overlying boundary layer of heated andesite, plumes of the
 484 bubble-laden basalt will tend to rise into the boundary layer of andesite owing to a Rayleigh-
 485 Taylor type instability once the rate of growth of the instability exceeds the rate of growth of
 486 the boundary layer (Thomas et al., 1993). For a boundary layer of thickness $h(t)$, the growth
 487 rate of the instability, σ , scales as

$$489 \quad \sigma \approx \frac{0.2g\Delta\rho h}{\mu_{sb}} \left(\frac{\mu_{sb}}{\mu_{bb}} \right)^{1/3} \quad (13)$$

490
 491 where μ_{sb} denotes the viscosity in the boundary layer of magma i , where $i = s$ or b . This
 492 exceeds the growth rate of the boundary layer, $\left(\frac{1}{h} \right) \frac{dh}{dt}$, which is driven by thermal
 493 conduction, $h \approx (\kappa_b t)^{1/2}$, when

$$495 \quad \frac{0.5g\Delta\rho h^3}{\kappa_b \mu_{sb}} \left(\frac{\mu_{sb}}{\mu_{bb}} \right)^{1/3} > 1 \quad (14)$$

496
 497 At this point, plumes of the cooled basalt will rise and mingle with the heated boundary layer
 498 of partially molten andesite. In **figure 6C**, we present an estimate of the thickness of the
 499 boundary layer at the point that this convective mingling is expected to become established
 500 and dominate the heat conduction within the boundary layer. Using the values for the reduced
 501 viscosity of the heated andesite, and values of the buoyancy of the basalt ranging from 50-
 502 150 kg/m³ (**figure 6C**), we estimate that the size of unstable boundary layer and hence the
 503 plumes of basalt which will mingle with the heated andesite are of order 3-6 cm,
 504 corresponding to times of order 0.1-1 days. Subsequently, as the boundary layer continues to
 505 deepen by heat conduction into the overlying andesite and the underlying hot basalt, the layer
 506 of mixed basalt and heated andesite will rise up into the cooler overlying andesite, once the
 507 rate of ascent of buoyant plumes through this cooler andesite is comparable to the rate of
 508 deepening of the boundary layer. Using comparable values for the buoyancy, but with the
 509 original viscosity of the crystalline andesite, 10⁶ to 10⁷ Pas, we estimate that such plumes will
 510 rise into the original andesite when the mixed layer has deepened to a scale of 10-25 cm, and

511 so will emerge from the boundary layer after the longer time of order 1-10 days. We therefore
512 envisage a two-stage process of convective intermingling within the boundary layer, followed
513 by the ascent of intermingled plumes from the boundary layer into the overlying andesite. We
514 also observe that if the upper layer of andesite is sufficiently crystalline, then the crystal-
515 crystal contacts may lead to the development of a yield stress in the upper layer, and this will
516 tend to suppress the ascent of plumes of buoyant melt into the main upper body of andesite,
517 whereas in the heated boundary layer, the crystal content will fall to lower values, thereby
518 reducing or eliminating this yield stress in the boundary layer itself. This additional effect
519 will again tend to promote an initial phase of local mixing in the boundary layer, and
520 provided the yield stress in the upper layer is not too large, this could then be followed by the
521 ascent of the mixed plumes into the upper layer once the buoyancy force associated with the
522 mixed layer exceeds the yield stress associated with the main body of andesite. Estimates of
523 yield stress in a crystalline magma suggest that it depends on the crystal shape and crystal
524 mass fraction (Hoover et al., 2001; Saar et al., 2001), but to allow mafic inclusions of size 0.1
525 m and buoyancy 100 kg/m^3 to rise through the melt, it should not exceed values of order 100
526 Pa, which is at the low end of the range. For larger values of yield stress, it may be that the
527 ascent of convective plumes into the upper layer would be restricted, further promoting the
528 mixing in the heated boundary layer. In that case, some limited intermingling of the hybrid
529 boundary layer into the overlying melt, and generation of mafic inclusions, might occur
530 during an eruptive phase, if the upper layer becomes mobilized by the larger scale stresses
531 driving the eruption. It is also relevant to note here that as bubbles are exsolved from the
532 basalt, the boundary layer in the basalt becomes less dense than the underlying basalt, and
533 hence stable to convective mixing into the main body of basalt (Cardoso and Woods, 1996).

534

535 **Conclusions**

536 Mafic enclaves erupted with crystal-rich andesite during the 1995-2011 eruption of Soufrière
537 Hills Volcano, Montserrat, display compositions and geochemical trends consistent with their
538 derivation at the interface between a basalt layer and an overlying andesite layer (**figure 7**).
539 The linear trends in major and trace element geochemistry of the mafic enclaves suggest that
540 they are formed by mixing between an end member tholeiitic basalt and the overlying
541 andesite, with the end member basalt changing in composition over time through the
542 eruption: becoming more primitive during phases I and III, then less primitive towards the
543 end of the eruption in phase V (**figure 5**). We propose that underplating vapor-saturated
544 mafic magma cools at the interface, and mixing with semi-molten andesite occurs in the

545 interface zone. The interface zone then becomes buoyant during cooling, mixing and
546 vesiculation and breaks off to form plumes, which rise into the overlying andesite. The mafic
547 enclaves become more primitive during phases I to III, which might be interpreted as being
548 due to quasi-continuous intrusion of increasingly primitive basalt from depth; it is certainly
549 not consistent with the continuous evolution of a basalt layer emplaced at the beginning of
550 the eruption which then evolves by cooling and crystallisation. After phase III, mafic
551 enclaves become more hybridised and larger, consistent with the cessation of intrusion of
552 mafic magma from depth, allowing the thermal diffusion front to migrate further into the
553 basalt, generating a thicker mixed boundary layer from which the enclaves form. It is worthy
554 of note that, from the analytical model we develop here, the timescales required to generate a
555 boundary layer of thickness similar to the dimension of mafic enclaves (decimetres) is on the
556 order of 1-10 days, which is similar to the timescales derived from diffusion profiles in
557 reverse-zoned phenocrysts and in Fe-Ti oxides both at Soufrière Hills (Devine et al., 1998)
558 and globally (Cooper and Kent, 2014). Quasi-continuous magma intrusion during 1995-2008
559 is consistent with continued high fluxes of SO₂ from Soufrière Hills (Edmonds et al., 2010)
560 and inflation of the volcano between eruptive phases (Elsworth et al., 2008).

561

562 Our analysis demonstrates that trends in mafic enclave geochemistry through an eruption
563 might yield insights into basalt underplating and its role in eruption triggering. The apparent
564 cessation of the eruption after phase V suggests that mafic magma intrusion may have played
565 a critical role in sustaining the eruption by heating and remobilising the overlying andesite
566 (Couch et al., 2001) and furthermore, this process and mechanism may be important at many
567 other arc volcanoes globally.

568

569 **Acknowledgements**

570 MP acknowledges a NERC studentship and University of Witwatersrand Postdoctoral
571 fellowship. MCSH was supported by a Royal Society University Research Fellowship.

572

573 **References**

- 574 Andersen, D.J., Lindsley, D.H., Davidson, P.M., 1993. QUILF: A pascal program to assess
575 equilibria among Fe Mg Mn Ti oxides, pyroxenes, olivine, and quartz. *Computers &*
576 *Geosciences* 19, 1333-1350.
- 577 Aspinall, W., Miller, A., Lynch, L., Latchman, J., Stewart, R., White, R., Power, J., 1998.
578 Soufrière Hills eruption, Montserrat, 1995–1997: Volcanic earthquake locations and fault
579 plane solutions. *Geophysical Research Letters* 25, 3397-3400.

580 Bachmann, O., Bergantz, G.W., 2006. Gas percolation in upper-crustal silicic crystal mushes
581 as a mechanism for upward heat advection and rejuvenation of near-solidus magma bodies.
582 *Journal of Volcanology and Geothermal Research* 149, 85-102.

583 Bacon, C.R., 1986. Magmatic inclusions in silicic and intermediate volcanic rocks. *Journal of*
584 *Geophysical Research: Solid Earth* 91, 6091-6112.

585 Barclay, J., Carroll, M., Rutherford, M., Murphy, M., Devine, J., Gardner, J., Sparks, R.,
586 1998. Experimental phase equilibria constraints on pre-eruptive storage conditions of the
587 Soufriere Hills magma. *Geophysical Research Letters*, 3437-3440.

588 Barclay, J., Herd, R.A., Edwards, B., Kiddle, E., Donovan, A., 2010. Caught in the act:
589 implications for the increasing abundance of mafic enclaves during the eruption of the
590 Soufriere Hills Volcano, Montserrat. *Geophysical Research Letters* 37.

591 Bergantz, G., Schleicher, J., Burgisser, A., 2015. Open-system dynamics and mixing in
592 magma mushes. *Nature Geoscience* 8, 793-796.

593 Browne, B.L., Eichelberger, J.C., Patino, L.C., Vogel, T.A., Uto, K., Hoshizumi, H., 2006.
594 Magma mingling as indicated by texture and Sr / Ba ratios of plagioclase phenocrysts from
595 Unzen volcano, SW Japan. *Journal of Volcanology and Geothermal Research* 154, 103-116.

596 Burgisser, A., Bergantz, G.W., 2011. A rapid mechanism to remobilize and homogenize
597 highly crystalline magma bodies. *Nature* 471, 212-215.

598 Cardoso, S.S., Woods, A.W., 1996. Interfacial turbulent mixing in stratified magma
599 reservoirs. *Journal of volcanology and geothermal research* 73, 157-175.

600 Cassidy, M., Edmonds, M., Watt, S.F., Palmer, M.R., Gernon, T.M., 2015. Origin of Basalts
601 by Hybridization in Andesite-dominated Arcs. *Journal of Petrology*, egv002.

602 Christopher, T., Blundy, J., Cashman, K., Cole, P., Edmonds, M., Smith, P., Sparks, R.,
603 Stinton, A., 2015. Crustal-scale degassing due to magma system destabilization and
604 magma-gas decoupling at Soufrière Hills Volcano, Montserrat. *Geochemistry, Geophysics,*
605 *Geosystems*.

606 Christopher, T., Edmonds, M., Humphreys, M., Herd, R.A., 2010. Volcanic gas emissions
607 from Soufrière Hills Volcano, Montserrat 1995–2009, with implications for mafic magma
608 supply and degassing. *Geophysical Research Letters* 37.

609 Christopher, T.E., Humphreys, M.C., Barclay, J., Genareau, K., De Angelis, S.M., Plail, M.,
610 Donovan, A., 2014. Petrological and geochemical variation during the Soufriere Hills
611 eruption, 1995 to 2010. *Geological Society, London, Memoirs* 39, 317-342.

612 Clyne, M.A., 1999. A Complex Magma Mixing Origin for Rocks Erupted in 1915, Lassen
613 Peak, California. *J. Petrology* 40, 105-132.

614 Coombs, M.L., Eichelberger, J.C., Rutherford, M.J., 2000. Magma storage and mixing
615 conditions for the 1953–1974 eruptions of Southwest Trident volcano, Katmai National Park,
616 Alaska. *Contr. Mineral. and Petrol.* 140, 99-118.

617 Cooper, K.M., Kent, A.J., 2014. Rapid remobilization of magmatic crystals kept in cold
618 storage. *Nature*.

619 Couch, S., Sparks, R., Carroll, M., 2001. Mineral disequilibrium in lavas explained by
620 convective self-mixing in open magma chambers. *Nature* 411, 1037-1039.

621 Davidson, J.P., Tepley, F.J., 1997. Recharge in volcanic systems: evidence from isotope
622 profiles of phenocrysts. *Science* 275, 826-829.

623 De Angelis, S.H., Larsen, J., Coombs, M., 2013. Pre-eruptive magmatic conditions at
624 Augustine Volcano, Alaska, 2006: evidence from amphibole geochemistry and textures.
625 *Journal of Petrology* 54, 1939-1961.

626 Devine, J., Murphy, M., Rutherford, M., Barclay, J., Sparks, R., Carroll, M., Young, S.,
627 Gardner, J., 1998. Petrologic evidence for pre-eruptive pressure-temperature conditions,
628 and recent reheating, of andesitic magma erupting at the Soufriere Hills Volcano, Montserrat,
629 WI. *Geophysical Research Letters* 25, 3669-3672.

630 Devine, J., Rutherford, M., Norton, G., Young, S., 2003. Magma storage region processes
631 inferred from geochemistry of Fe–Ti oxides in andesitic magma, Soufriere Hills Volcano,
632 Montserrat, WI. *Journal of Petrology* 44, 1375-1400.

633 Edmonds, M., Aiuppa, A., Humphreys, M., Moretti, R., Giudice, G., Martin, R., Herd, R.,
634 Christopher, T., 2010. Excess volatiles supplied by mingling of mafic magma at an andesite
635 arc volcano. *Geochemistry, Geophysics, Geosystems* 11.

636 Edmonds, M., Humphreys, M.C., Hauri, E.H., Herd, R.A., Wadge, G., Rawson, H., Ledden,
637 R., Plail, M., Barclay, J., Aiuppa, A., 2014. Pre-eruptive vapour and its role in controlling
638 eruption style and longevity at Soufrière Hills Volcano. Geological Society, London,
639 *Memoirs* 39, 291-315.

640 Edmonds, M., Pyle, D., Oppenheimer, C., 2001. A model for degassing at the Soufrière Hills
641 Volcano, Montserrat, West Indies, based on geochemical data. *Earth and Planetary Science*
642 *Letters* 186, 159-173.

643 Eichelberger, J.C., Chertkoff, D.G., Dreher, S.T., Nye, C.J., 2000. Magmas in collision:
644 rethinking chemical zonation in silicic magmas. *Geology* 28, 603-606.

645 Elsworth, D., Mattioli, G., Taron, J., Voight, B., Herd, R., 2008. Implications of magma
646 transfer between multiple reservoirs on eruption cycling. *Science* 322, 246-248.

647 Ghiorso, M., Sack, R., 1995. Chemical mass transfer in magmatic processes IV. A revised
648 and internally consistent thermodynamic model for the interpolation and extrapolation of
649 liquid-solid equilibria in magmatic systems at elevated temperatures and pressures. *Contr.*
650 *Mineral. and Petrol.* 119, 197-212.

651 Ghiorso, M.S., Gualda, G.A., 2015. An H₂O–CO₂ mixed fluid saturation model compatible
652 with rhyolite-MELTS. *Contr. Mineral. and Petrol.* 169, 1-30.

653 Holland, T., Blundy, J., 1994. Non-ideal interactions in calcic amphiboles and their bearing
654 on amphibole-plagioclase thermometry. *Contr. Mineral. and Petrol.* 116, 433-447.

655 Hoover, S., Cashman, K., Manga, M., 2001. The yield strength of subliquidus basalts—
656 experimental results. *Journal of Volcanology and Geothermal Research* 107, 1-18.

657 Huber, C., Bachmann, O., Dufek, J., 2011. Thermo-mechanical reactivation of locked crystal
658 mushes: Melting-induced internal fracturing and assimilation processes in magmas. *Earth and*
659 *Planetary Science Letters* 304, 443-454.

660 Humphreys, M., Edmonds, M., Christopher, T., Hards, V., 2009a. Chlorine variations in the
661 magma of Soufrière Hills Volcano, Montserrat: Insights from Cl in hornblende and melt
662 inclusions. *Geochimica et Cosmochimica Acta* 73, 5693-5708.

663 Humphreys, M., Edmonds, M., Christopher, T., Hards, V., 2010. Magma hybridisation and
664 diffusive exchange recorded in heterogeneous glasses from Soufrière Hills Volcano,
665 Montserrat. *Geophysical Research Letters* 37.

666 Humphreys, M., Edmonds, M., Plail, M., Barclay, J., Parkes, D., Christopher, T., 2013. A
667 new method to quantify the real supply of mafic components to a hybrid andesite. *Contr.*
668 *Mineral. and Petrol.* 165, 191-215.

669 Humphreys, M.C., Christopher, T., Hards, V., 2009b. Microlite transfer by disaggregation of
670 mafic inclusions following magma mixing at Soufrière Hills volcano, Montserrat. *Contr.*
671 *Mineral. and Petrol.* 157, 609-624.

672 Klemetti, E.W., Clynne, M.A., 2014. Localized rejuvenation of a crystal mush recorded in
673 zircon temporal and compositional variation at the Lassen Volcanic Center, Northern
674 California. *PLoS One* 9, e113157.

675 Komorowski, J.C., Legendre, Y., Christopher, T., Bernstein, M., Stewart, R., Joseph, E.,
676 Fournier, N., Chardot, L., Finizola, A., Wadge, G., 2010. Insights into processes and deposits
677 of hazardous vulcanian explosions at Soufrière Hills Volcano during 2008 and 2009
678 (Montserrat, West Indies). *Geophysical Research Letters* 37.

679 Laumonier, M., Scaillet, B., Pichavant, M., Champallier, R., Andujar, J., Arbaret, L., 2014.
680 On the conditions of magma mixing and its bearing on andesite production in the crust.
681 Nature communications 5.

682 Mann, C.P., Wallace, P.J., Stix, J., 2013. Phenocryst-hosted melt inclusions record stalling of
683 magma during ascent in the conduit and upper magma reservoir prior to vulcanian
684 explosions, Soufrière Hills volcano, Montserrat, West Indies. Bull Volcanol 75, 687.

685 Martin, V.M., Pyle, D.M., Holness, M.B., 2006. The role of crystal frameworks in the
686 preservation of enclaves during magma mixing. Earth and Planetary Science Letters 248,
687 787-799.

688 Miyashiro, A., 1974. Volcanic rock series in island arcs and active continental margins.
689 American journal of science 274, 321-355.

690 Murphy, M., Sparks, R., Barclay, J., Carroll, M., Brewer, T., 2000. Remobilization of
691 andesite magma by intrusion of mafic magma at the Soufriere Hills Volcano, Montserrat,
692 West Indies. Journal of petrology 41, 21-42.

693 Murphy, M., Sparks, R., Barclay, J., Carroll, M., Lejeune, A., Brewer, T., MacDonald, R.,
694 Black, S., 1998. The role of magma mixing in triggering the current eruption at the Soufriere
695 Hills Volcano, Montserrat. Geophysical Research Letters, 3433-3436.

696 Nakagawa, M., Wada, K., Wood, C.P., 2002. Mixed magmas, mush chambers and eruption
697 triggers: evidence from zoned clinopyroxene phenocrysts in andesitic scoria from the 1995
698 eruptions of Ruapehu volcano, New Zealand. Journal of petrology 43, 2279-2303.

699 Nakamura, M., 1995. Continuous mixing of crystal mush and replenished magma in the
700 ongoing Unzen eruption. Geology 23, 807-810.

701 Phillips, J.C., Woods, A.W., 2002. Suppression of large-scale magma mixing by melt-
702 volatile separation. Earth and Planetary Science Letters 204, 47-60.

703 Plail, M., Barclay, J., Humphreys, M.C., Edmonds, M., Herd, R.A., Christopher, T.E., 2014.
704 Characterization of mafic enclaves in the erupted products of Soufrière Hills Volcano,
705 Montserrat, 2009 to 2010. Geological Society, London, Memoirs 39, 343-360.

706 Reagan, M.K., Gill, J.B., Malavassi, E., Garcia, M.O., 1987. Changes in magma composition
707 at Arenal volcano, Costa Rica, 1968–1985: real-time monitoring of open-system
708 differentiation. Bull Volcanol 49, 415-434.

709 Reubi, O., Blundy, J., 2009. A dearth of intermediate melts at subduction zone volcanoes and
710 the petrogenesis of arc andesites. Nature 461, 1269-1273.

711 Rudnick, R.L., 1995. Making continental crust. Nature 378, 571.

712 Ruprecht, P., Bachmann, O., 2010. Pre-eruptive reheating during magma mixing at Quizapu
713 volcano and the implications for the explosiveness of silicic arc volcanoes. Geology 38, 919-
714 922.

715 Rutherford, M.J., Devine, J.D., 2003. Magmatic conditions and magma ascent as indicated by
716 hornblende phase equilibria and reactions in the 1995–2002 Soufriere Hills magma. Journal
717 of Petrology 44, 1433-1453.

718 Saar, M.O., Manga, M., Cashman, K.V., Fremouw, S., 2001. Numerical models of the onset
719 of yield strength in crystal–melt suspensions. Earth and Planetary Science Letters 187, 367-
720 379.

721 Shepherd, J., Tomblin, J., Woo, D., 1971. Volcano-seismic crisis in Montserrat, West Indies,
722 1966–67. Bulletin volcanologique 35, 143-162.

723 Singer, B.S., Dungan, M.A., Layne, G.D., 1995. Textures and Sr, Ba, Mg, Fe, K, and Ti
724 compositional profiles in volcanic plagioclase: clues to the dynamics of calc-alkaline magma
725 chambers. American Mineralogist 80, 776-798.

726 Sparks, R., Marshall, L., 1986. Thermal and mechanical constraints on mixing between mafic
727 and silicic magmas. Journal of Volcanology and Geothermal Research 29, 99-124.

728 Sparks, R.S.J., Young, S.R., Barclay, J., Calder, E.S., Cole, P., Darroux, B., Davies, M.,
729 Druitt, T., Harford, C., Herd, R., 1998. Magma production and growth of the lava dome of
730 the Soufriere Hills Volcano, Montserrat, West Indies: November 1995 to December 1997.
731 *Geophysical Research Letters* 25, 3421-3424.
732 Sun, S.-S., McDonough, W.-s., 1989. Chemical and isotopic systematics of oceanic basalts:
733 implications for mantle composition and processes. *Geological Society, London, Special*
734 *Publications* 42, 313-345.
735 Tepley, F., Davidson, J., Clyne, M., 1999. Magmatic interactions as recorded in plagioclase
736 phenocrysts of Chaos Crags, Lassen Volcanic Center, California. *Journal of Petrology* 40,
737 787-806.
738 Thomas, N., Tait, S., Koyaguchi, T., 1993. Mixing of stratified liquids by the motion of gas
739 bubbles: application to magma mixing. *Earth and Planetary Science Letters* 115, 161-175.
740 Victoria, V., Morgan, D., Jerram, D., Caddick, M., Prior, D., Davidson, J., 2008. Bang!
741 Month-scale eruption triggering at Santorini volcano. *Science* 321, 1178-1178.
742 Vogel, T.A., Hidalgo, P.J., Patino, L., Tefend, K.S., Ehrlich, R., 2008. Evaluation of magma
743 mixing and fractional crystallization using whole-rock chemical analyses: Polytopic vector
744 analyses. *Geochemistry, Geophysics, Geosystems* 9.
745 Wadge, G., Voight, B., Sparks, R., Cole, P., Loughlin, S., Robertson, R., 2014. An overview
746 of the eruption of Soufriere Hills Volcano, Montserrat from 2000 to 2010. *Geological*
747 *Society, London, Memoirs* 39, 1-40.
748 White, W., Copeland, P., Gravatt, D.R., Devine, J.D., 2017. Geochemistry and
749 geochronology of Grenada and Union islands, Lesser Antilles: The case for mixing between
750 two magma series generated from distinct sources. *Geosphere* 13, 1359-1391.
751 Woods, A.W., Cowan, A., 2009. Magma mixing triggered during volcanic eruptions. *Earth*
752 *and Planetary Science Letters* 288, 132-137.
753 Zellmer, G., Hawkesworth, C., Sparks, R., Thomas, L., Harford, C., Brewer, T., Loughlin, S.,
754 2003a. Geochemical evolution of the Soufriere Hills volcano, Montserrat, Lesser Antilles
755 volcanic arc. *Journal of Petrology* 44, 1349-1374.
756 Zellmer, G., Sparks, R., Hawkesworth, C., Wiedenbeck, M., 2003b. Magma emplacement
757 and remobilization timescales beneath Montserrat: insights from Sr and Ba zonation in
758 plagioclase phenocrysts. *Journal of Petrology* 44, 1413-1431.
759 Zellmer, G.F.H., C. J. Sparks, R. S. J. Thomas, L. E. Harford, C. L. Brewer, T. S. Loughlin,
760 S. C., 2003. Geochemical Evolution of the Soufrière Hills Volcano, Montserrat, Lesser
761 Antilles Volcanic Arc. *Journal of Petrology* 44, 1349 -1374.

762

763

764 **Table and figures**

765

<i>Phase I</i>	<i>Phase II</i>	<i>Phase III</i>	<i>Phase IV</i>	<i>Phase V</i>
Nov. 95 – Mar. 98	Nov. 99 – Jul. 03	Aug. 05 – Apr. 07	Jul. 08 – Jan. 09	Oct. 09 – Feb. 10

766

767 **Table 1:** Soufrière Hills Volcano (Montserrat) eruption phases (Wadge et al., 2014).

768

769 **Figure 1:** A: Map of Montserrat showing the location of the Soufrière Hills Volcano. B:
770 photomicrograph of a mafic inclusion, showing a typical diktytaxitic texture made up of

771 blocky plagioclase and dark brown amphibole crystals. Light brown glass surrounds the
772 crystals. C: photomicrograph of the interface between crystal-rich andesite (top) and mafic
773 inclusion (bottom). Orthopyroxene and magnetite are visible in the mafic enclave. The
774 andesite has a highly crystalline groundmass. D: an image of a typical andesitic block on
775 outcrop scale with mafic enclaves from phase V block and ash deposits in the Belham Valley,
776 Montserrat.

777

778 **Figure 2:** Major element compositions of whole rock lavas (solid circles) and glasses
779 (crosses) from the Soufrière Hills eruption, phases I to V (see legend) (Barclay et al., 2010;
780 Mann et al., 2013; Murphy et al., 2000; Plail et al., 2014; Zellmer, 2003). Also shown are
781 lava compositions from South Soufrière Hills (Cassidy et al., 2015). A: MgO versus SiO₂, in
782 wt%; B: Al₂O₃ versus SiO₂, in wt%; C: CaO versus SiO₂, in wt%; D: K₂O versus SiO₂, in
783 wt% and E: FeO_{tot}/MgO versus SiO₂, in wt%. Tholeiite (TH) and calc-alkaline (CA) fields
784 are marked. Fractional crystallisation trends from Rhyolite Melts (Ghiorso and Gualda, 2015)
785 are shown.

786

787 **Figure 3:** Trace element plot to show lava compositions from phases 1 to V of the Soufrière
788 Hills Volcano eruption. Data from this work and from Zellmer (2003). Trace element
789 compositions normalised to primitive mantle (*Sun and McDonough, 1989*).

790

791 **Figure 4:** Trace element compositions of whole rock lavas from the Soufrière Hills eruption,
792 phases I to V (see legend) from this work and *Zellmer [2003]*. A: Dy versus La, in ppm; B:
793 Yb versus La, in ppm; C: V versus La, in ppm; D: Sc versus La, in ppm; E: Sr versus La, in
794 ppm. Vectors to show the effect of 20% fractionation of various crystal phases are shown (for
795 method and partition coefficients used see **Supplementary Material**). Mixing lines are
796 shown on the V vs La plot, showing the amount of mixing required to form the array of mafic
797 enclaves for mixing between an end member basalt and the most evolved andesite bulk
798 composition. To generate the most Si-rich mafic enclave erupted in phase V requires mixing
799 67% andesite and 33% basalt; fits and residuals for each element are given in
800 **Supplementary Table 3**.

801

802 **Figure 5:** Box and whisker plots to show Mg/Fe and V/La over the five phases of the
803 eruption. The box is bounded by the 75th and 25th quartile values, with a horizontal line
804 through the box denoting the median. Whiskers show the minimum and maximum values.

805 Mafic enclave compositions are shown in blue; andesite in red. Below is a timeline to show
806 when eruptive phases occurred and interpretative labelling (see main text discussion for
807 justification).

808

809 **Figure 6:** A model to describe the interaction between basalt magma and overlying andesite.
810 A: Thermal profile across the boundary between basalt and andesite after 1 and 10 days; B:
811 how the buoyancy (density difference between the boundary layer and the overlying andesite)
812 varies during cooling and crystallisation, for two water contents (2 and 4 wt%); C: the
813 variation of the scale of the plume rising from the boundary layer with viscosity of the
814 boundary layer magma, for various boundary layer buoyancy values. A more buoyant
815 boundary layer is expected to form smaller mafic enclaves.

816

817 **Figure 7:** Schematic diagram to illustrate the controls on mafic enclave composition and how
818 it may evolve with time. Left: vapor-saturated mafic magma (basalt) underplates a reservoir
819 of crystal-rich andesite containing a range of crystal phases (pl: plagioclase; opx:
820 orthopyroxene; am: amphibole). An initially thin hybrid boundary layer forms as the basalt
821 quench-cools and crystallises while the andesite partially melts, allowing them to mix in this
822 layer. Middle: When the buoyancy of the layer is sufficient buoyant plumes form at the
823 interface, which rise into the heated lower viscosity layer of andesite and form mafic
824 enclaves, which may be stirred into the heated andesite and which have a dimension similar
825 to the thickness of the boundary layer. Quenched-rim basaltic mafic inclusions are among the
826 first to break off from the interface. Composite enclaves may form from hybrid material
827 surrounded by more mafic material as the latter rises up in the wake of boundary layer break-
828 up. Initially the proportion of mafic material is small (~1 vol% (Barclay et al., 2010)). Right:
829 if the intrusion of mafic magma is shut off and the basalt cools, the boundary layer will grow
830 by thermal diffusion, the mafic enclaves will become larger, and there will be a higher
831 volume proportion of mafic enclaves in the erupted lavas, as has been observed (Barclay et
832 al., 2010).

833

834

835

<i>Phase I</i>	<i>Phase II</i>	<i>Phase III</i>	<i>Phase IV</i>	<i>Phase V</i>
Nov. 95 – Mar. 98	Nov. 99 – Jul. 03	Aug. 05 – Apr. 07	Jul. 08 – Jan. 09	Oct. 09 – Feb. 10

Table 1: Soufrière Hills Volcano (Montserrat) eruption phases (Wadge et al., 2014).

Figure 1

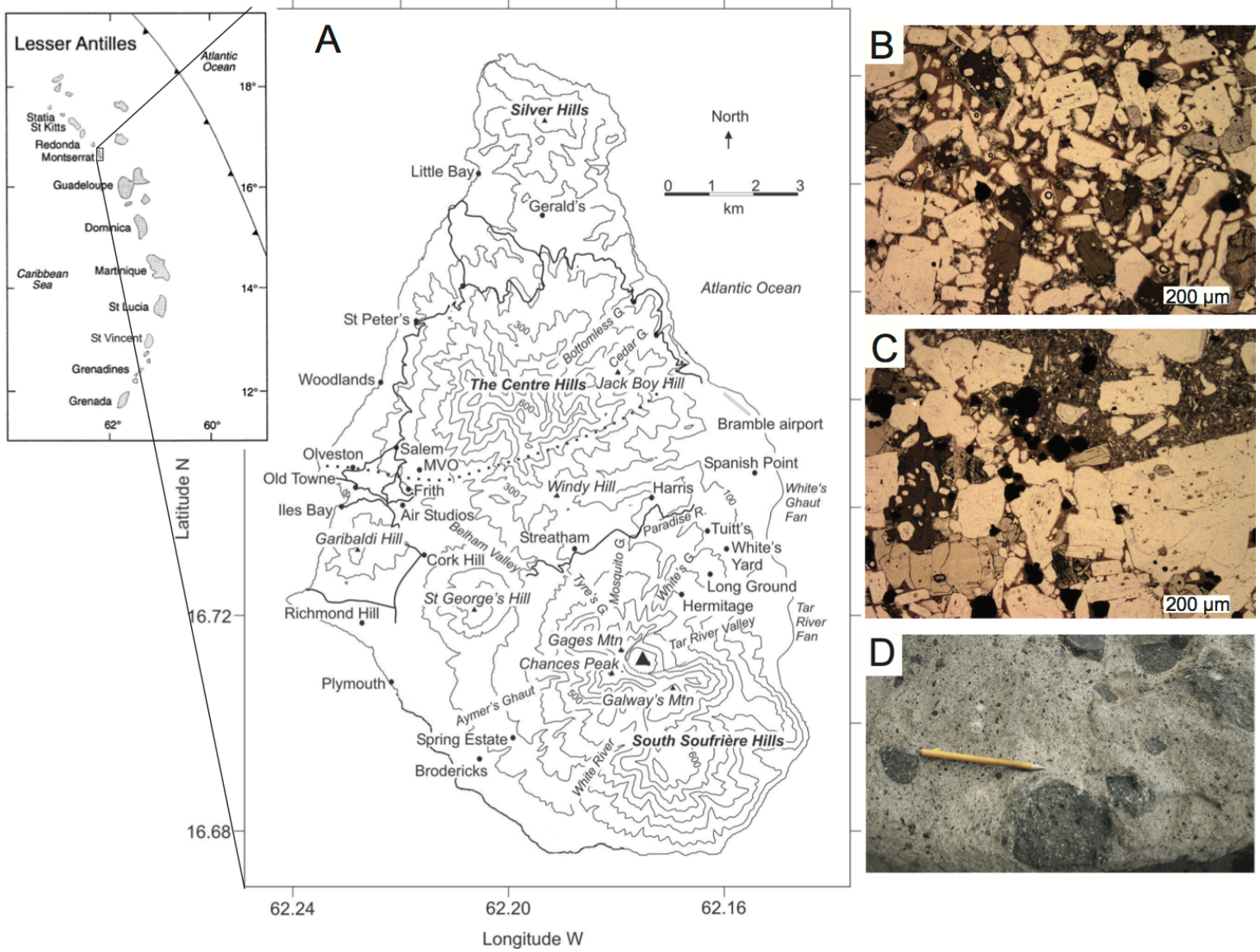


Figure 2

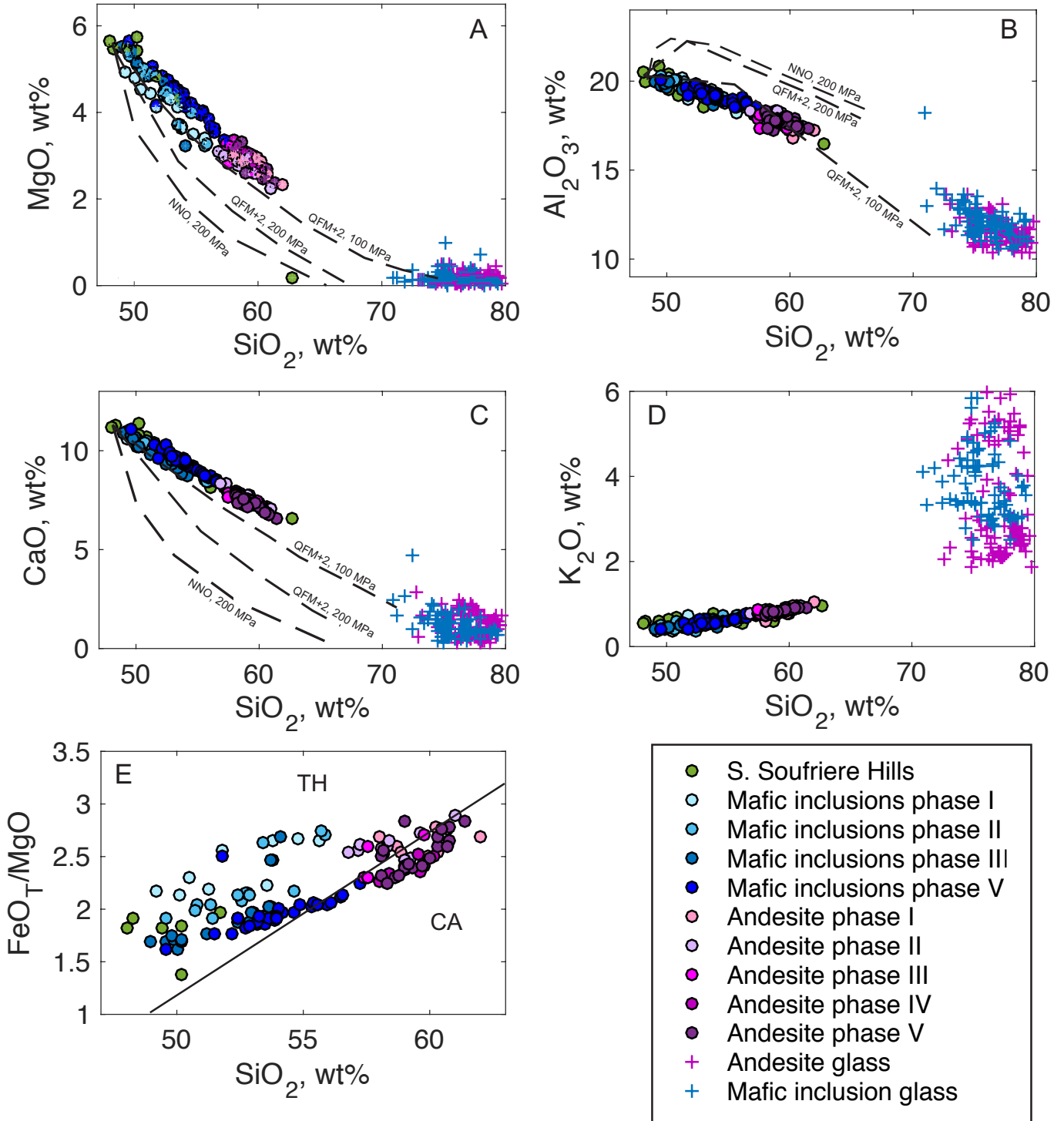


Figure 3

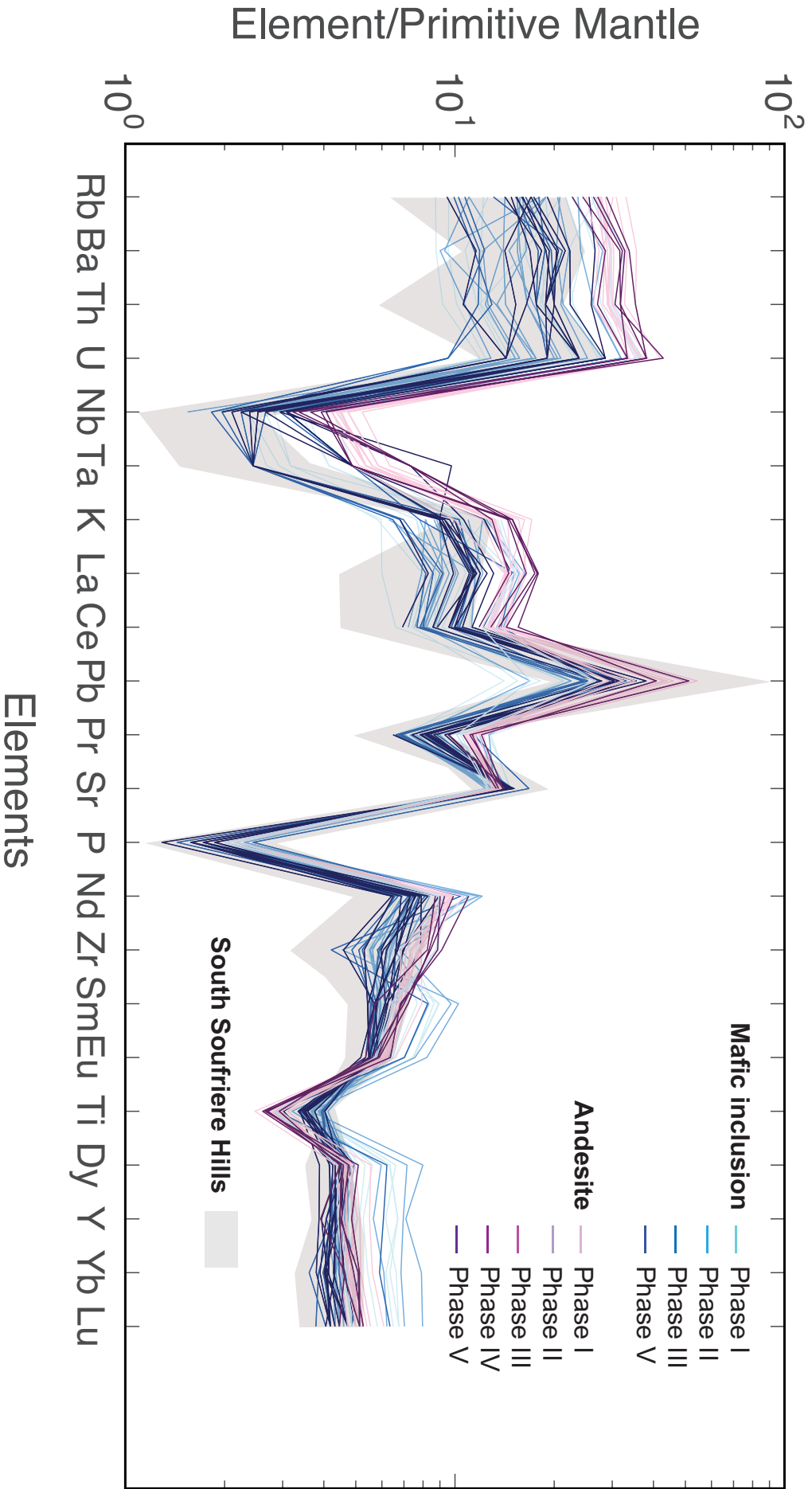


Figure 4

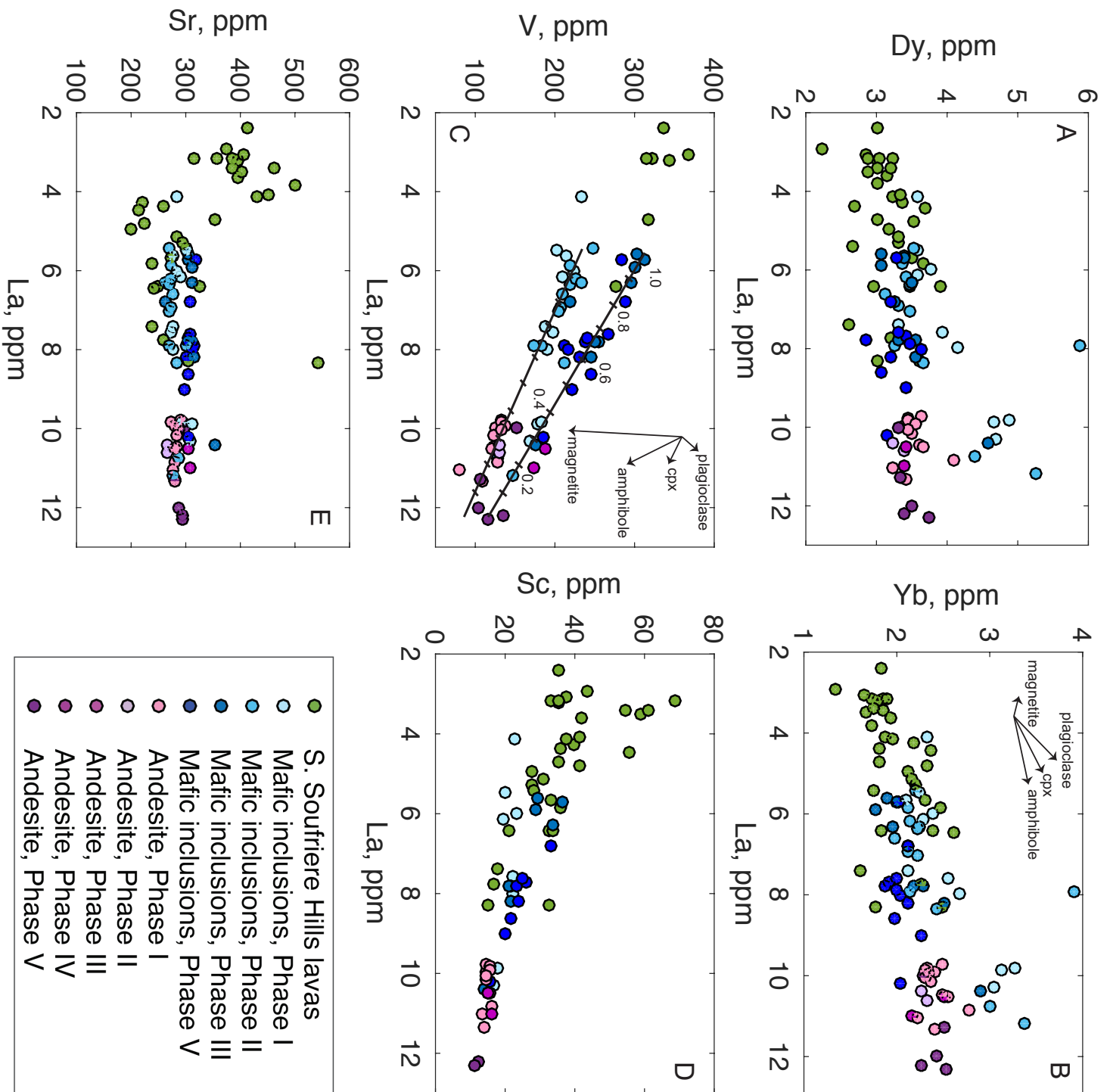


Figure 5

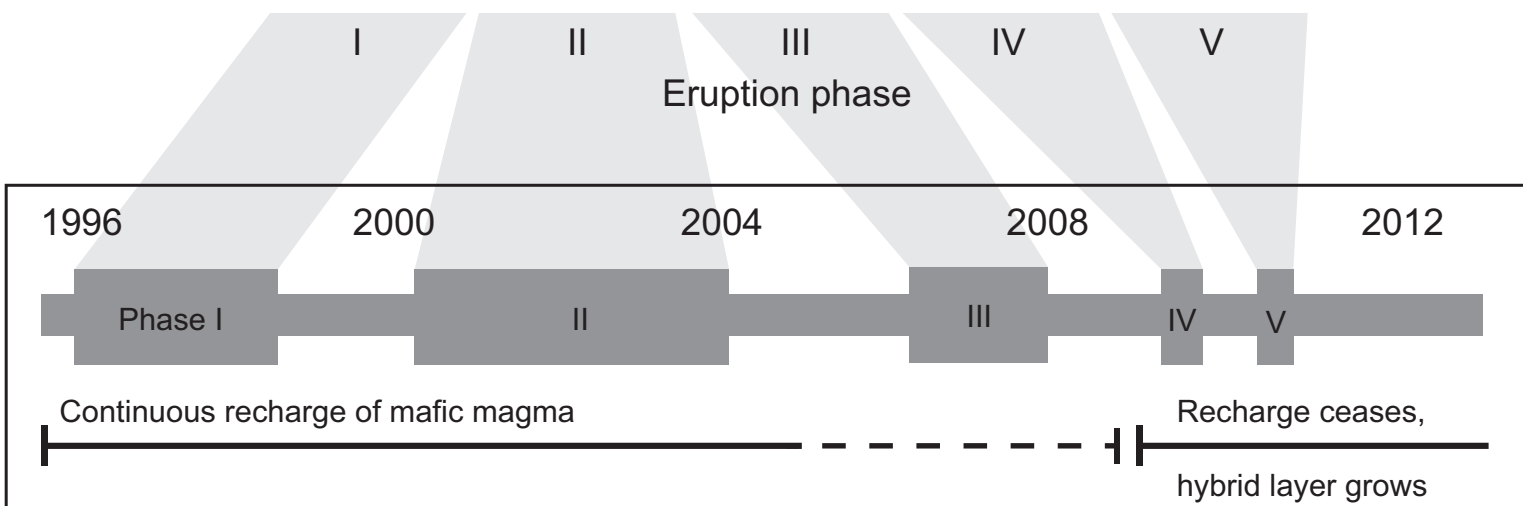
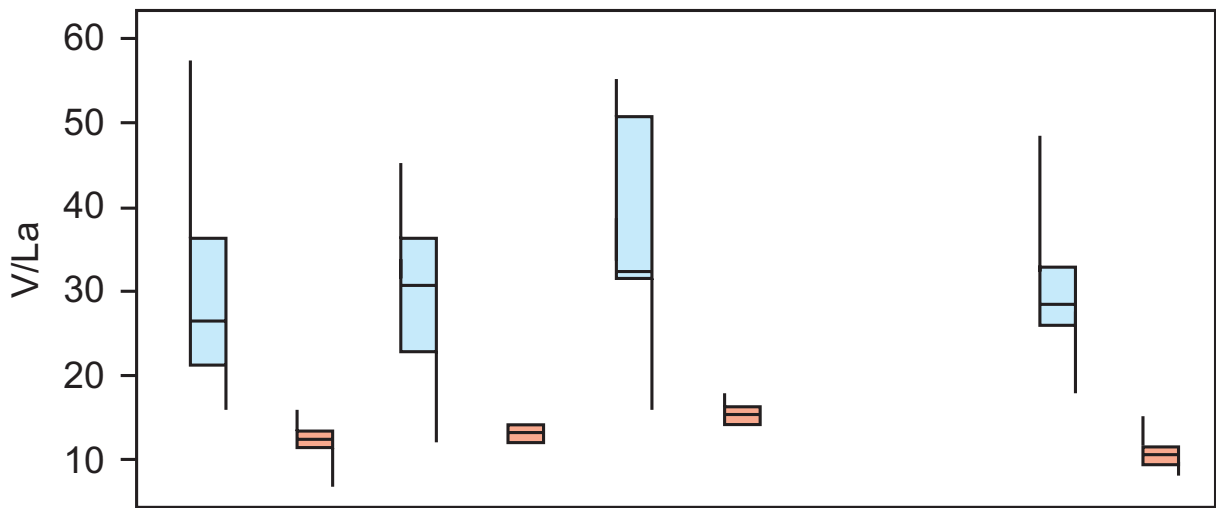
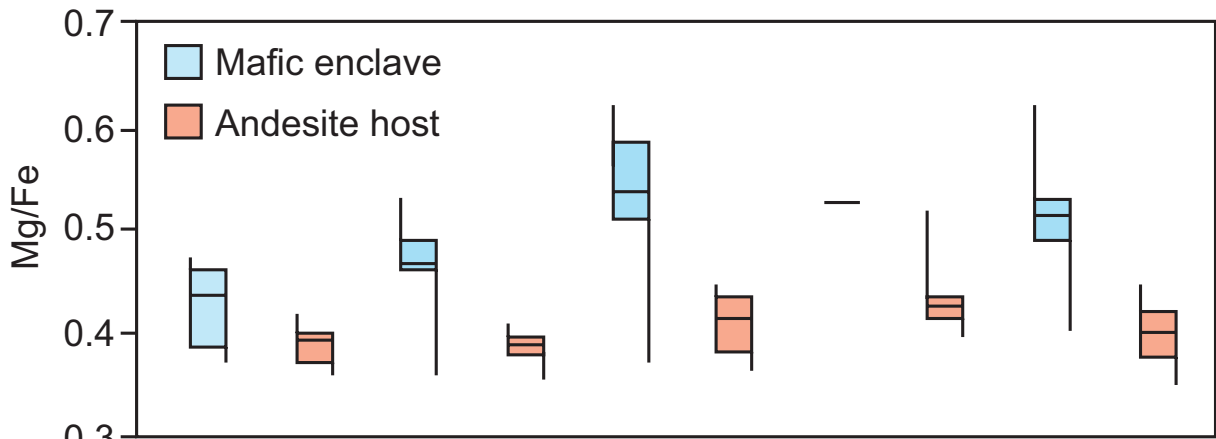


Figure 6

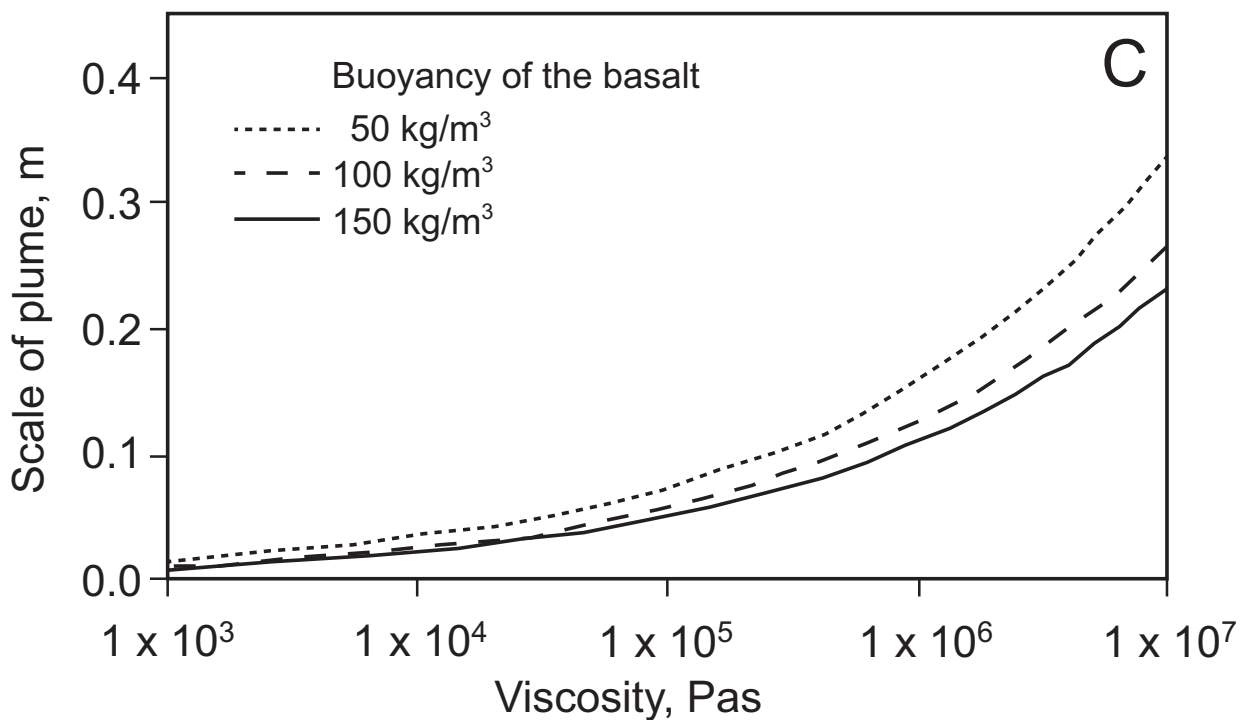
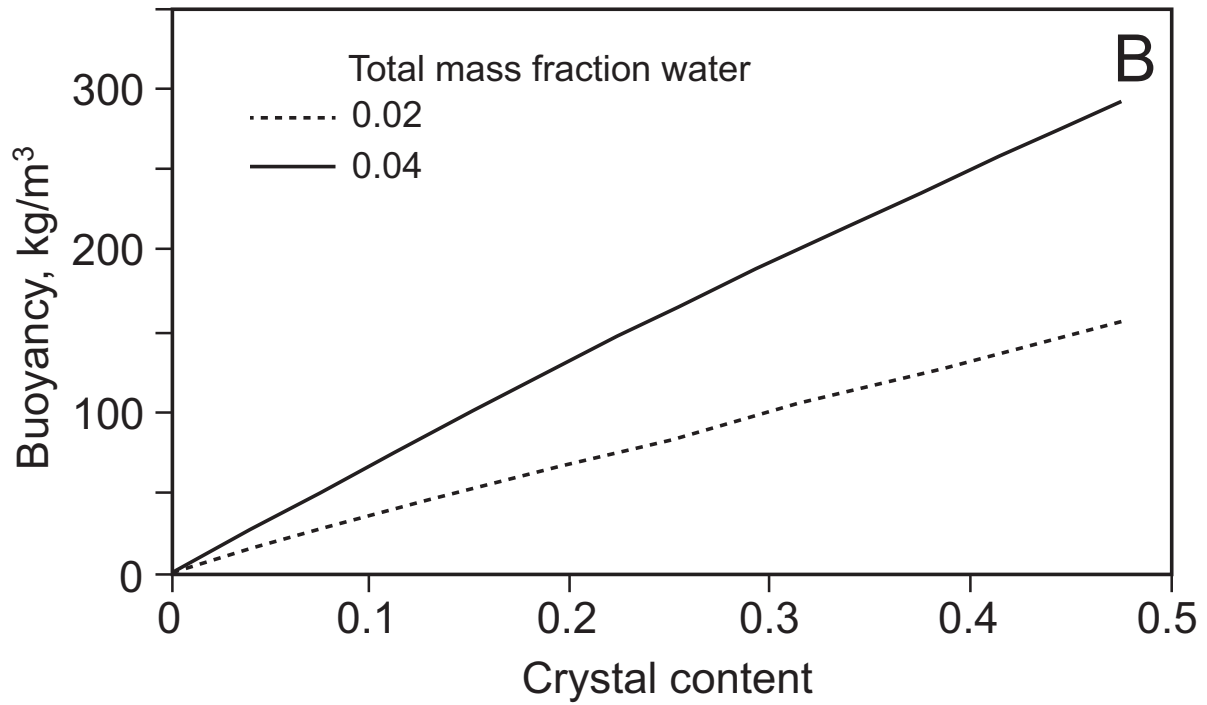
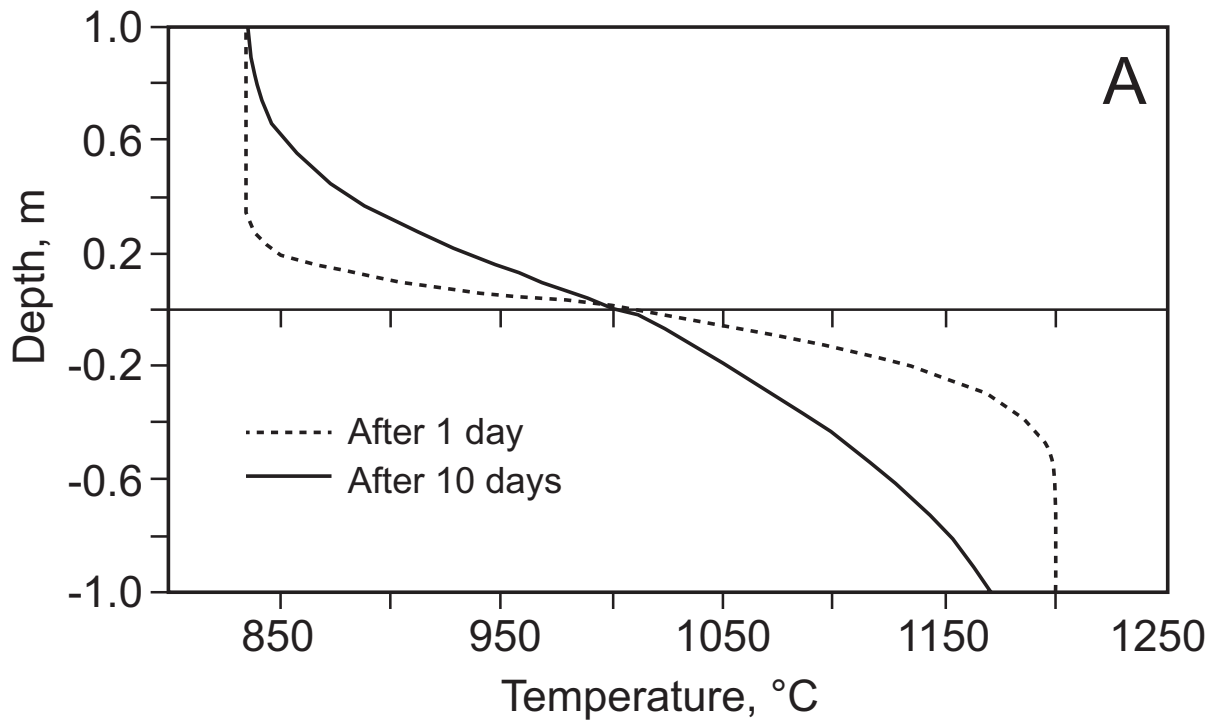


Figure 7

